JOC The Journal of Organic Chemistry

pubs.acs.org/joc Article

Axial Chirality around N−P Bonds Induced by Complexation between $E(C_6F_5)_3$ (E = B, Al) and an *N*-Phosphine Oxide-Substituted Imidazolinylidene: A Key Intermediate in the Catalytic Phosphinoylation of CO_2

Takahiro Asada, Yoichi Hoshimoto,* Takahiro Kawakita, Takuya Kinoshita, and Sensuke Ogoshi*

Cite This: *J. Org. Chem.* 2020, 85, 14333−14341 Read Online

ACCESS | Metrics & More | Article Recommendations | Supporting Information

ABSTRACT: Complexation-induced axial chirality around an N−P bond occurs upon the predominant coordination of the *N*-phosphinoyl group in the *N*-phosphine oxide-substituted imidazolinylidene (SPoxIm) to $B(C_6F_5)_3$. (R_a) and (S_a) atropisomers of (κ-*O*-SPoxIm)$B(C_6F_5)_3$ were observed independently in the single-crystal lattice and the optimized gas-phase structure. Experimental and theoretical studies confirmed that this axial chirality arises from the restricted rotation around the N−P bond, caused by the steric repulsion between the C5−H atoms of the imidazolinylidene ring and the C_6F_5 rings on the $B(C_6F_5)_3$ unit. Conversely, this axial chirality was not certainly observed via the complexation between SPoxIm and $Al(C_6F_5)_3$. The carbene carbon atoms in (κ-*O*-SPoxIm)$E(C_6F_5)_3$ (E = B, Al) remain sufficiently nucleophilic to react with CO_2, and the phosphinoylation of CO_2 with SPoxIm proceeds far more rapidly in the presence of a catalytic amount of $Al(C_6F_5)_3$ than in the absence of $Al(C_6F_5)_3$.

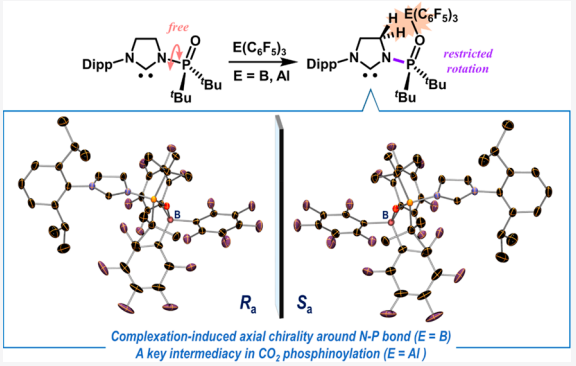

INTRODUCTION

Over the past decades, numerous applications have been developed for *N*-heterocyclic carbenes (NHCs) in diverse areas of chemistry.[1] Multifunctional NHCs equipped with additional coordination sites have further diversified the structures and functions of NHCs; however, their utility has been majorly limited to serve as multidentate ligands for the complexation of metals.[2] Thus, exploring the unprecedented utility of multifunctional NHCs would significantly advance the development of NHC chemistry.

Recently, we have proposed a concept of multifunctional multipurpose carbenes,[3] i.e., carbenes that include functional groups applicable to a variety of purposes beyond additional coordination sites. In this context, *N*-phosphine oxide-substituted imidazolylidene (PoxIm) and the corresponding imidazolinylidene (SPoxIm) represent pioneering examples (Figure 1A). Under ambient conditions, (S)PoxIms predominantly exist in the *anti*-conformation ($\theta \approx 0°$; θ is defined as shown in Figure 1A), in which the carbene carbon and the phosphinoyl oxygen atoms adopt an *anti*-orientation with respect to the N−P bond. Rotation of the *N*-phosphinoyl moiety to generate the *syn*-conformer ($\theta \approx 160°$) can occur via a relatively low energy barrier to overcome TS ($\theta \approx 90°$; $\Delta E^{\ddagger} \approx 12$ kcal·mol^{-1} for previously reported PoxIms).[3a] The *N*-phosphinoyl groups in PoxIms were used for scaling the

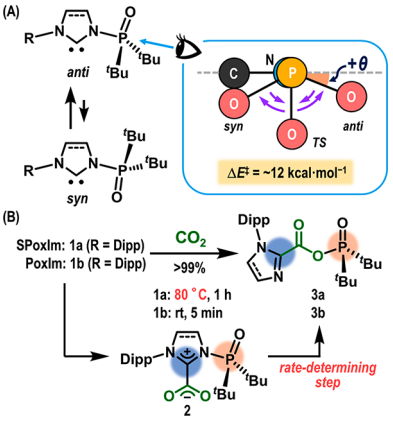

Figure 1. (A) Interconversion between *anti*- and *syn*-conformers of *N*-phosphine oxide-substituted imidazolylidene (PoxIm) and imidazolinylidene (SPoxIm). (B) Previously reported phosphinoylation of CO_2 with SPoxIm (**1a**) and PoxIm (**1b**). Dipp, *N*-2,6-$^{i}Pr_2C_6H_3$.

Special Issue: The New Golden Age of Organophosphorus Chemistry

Received: November 28, 2019
Published: January 3, 2020

https://dx.doi.org/10.1021/acs.joc.9b03210
J. Org. Chem. 2020, 85, 14333−14341

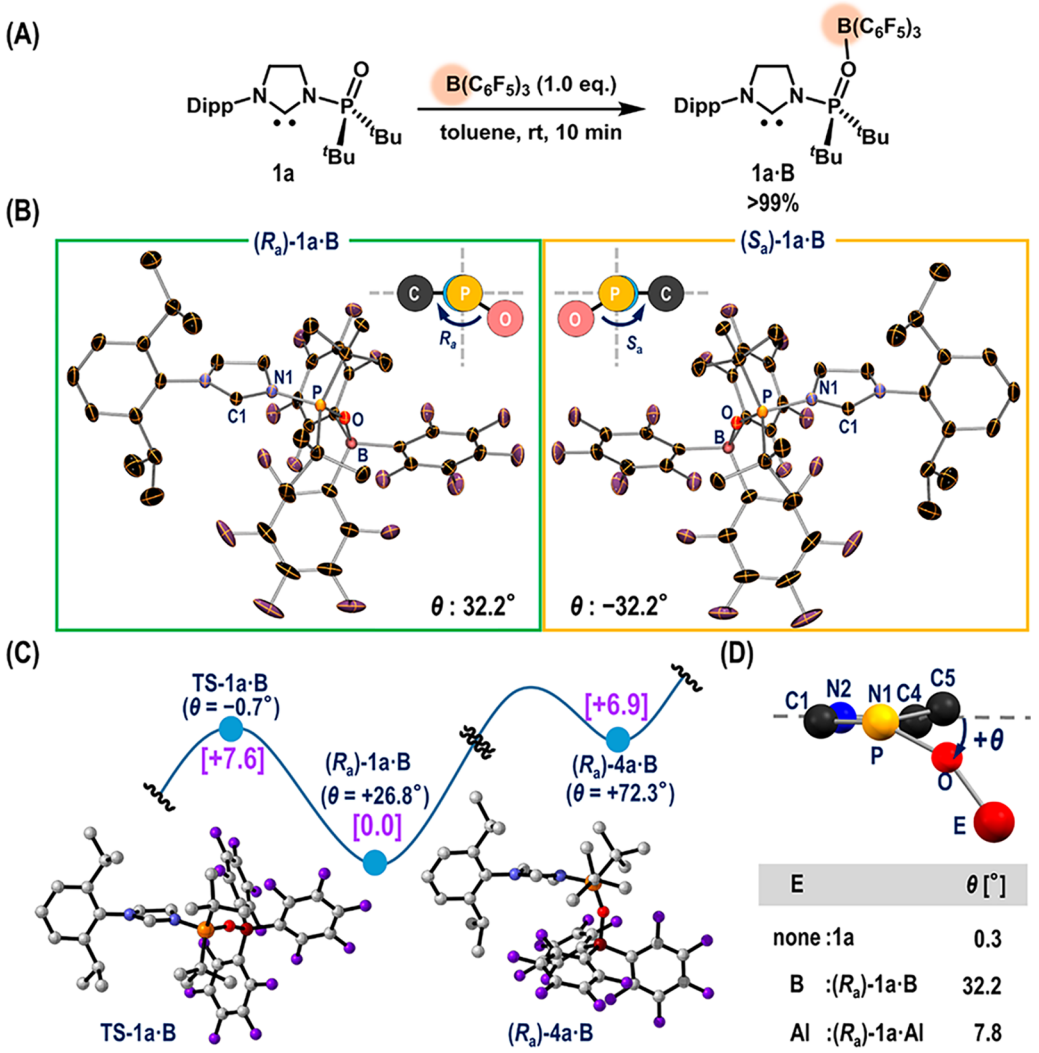

Figure 2. (A) Synthesis of **1a·B** from **1a** and $B(C_6F_5)_3$. The yield of the isolated product is shown. (B) Molecular structures of (R_a)-**1a·B** (left) and (S_a)-**1a·B** (right) with thermal ellipsoids at 30% probability; H atoms are omitted for clarity. Selected bond lengths (Å) and angles (deg) in (R_a)-**1a·B**: N1−P 1.666(1), P−O 1.525(1), O−B 1.551(2), P−O−B 154.43(8), C1−N1−P−O + 147.8(1) (C) The relative Gibbs free energies (kcal·mol^{-1}) for **TS-1a·B** and (R_a)-**4a·B** with respect to (R_a)-**1a·B** (+0.0 kcal·mol^{-1}), and their angles of θ. The optimized gas phase structures of **TS-1a·B** (left) and (R_a)-**4a·B** (right) are also shown. Gray, C; blue, N; orange, P; red, O; brown, B; purple, F. Selected bond lengths (Å) and angles (deg): **TS-1a·B**; N1−P 1.69, P−O 1.54, O−B 1.58, P−O−B 160.8, C1−N1−P-O −179.3. (R_a)-**4a·B**; N1−P 1.69, P−O 1.54, O−B 1.57, P−O−B 154.2, C1−N1−P-O + 107.7. (D) Comparison on the angles of θ between molecular structures of **1a**, (R_a)-**1a·B**, and (R_a)-**1a·Al**, determined by the single-crystal XRD analyses.

coordination sphere around the carbene carbon via rotation around the N−P bond,[3a] as well as for the phosphinoylation of CO_2, which is enabled by cooperation between the nucleophilic carbene carbon and the electrophilic phosphorus atoms.[3b] The latter was applied to the straightforward, one-pot synthesis of carbonyl compounds, including challenging unsymmetrical ketones, from gaseous CO_2. However, the reaction between CO_2 and SPoxIm (**1a**) or PoxIm (**1b**), both of which bear a *N*-2,6-^{i}Pr$_2$C$_6$H$_3$ (Dipp) group, was far faster for the latter than the former, and heating was required to expedite the reaction with **1a** (Figure 1B). Detailed mechanistic studies uncovered that the N to O migration of the phosphinoyl moiety in imidazolium-2-carboxylate intermediates **2** is involved in the rate-determining event. We thus envisioned a promotion of this migration step via an enhancement of the electrophilicity on the phosphorus atom in **2** by the predominant complexation between the *N*-phosphinoyl group in SPoxIm and Lewis acids. Herein, we report a significant acceleration of the phosphinoylation of CO_2 with SPoxIm in the presence of a catalytic amount of $Al(C_6F_5)_3$. A potential intermediacy of (κ-*O*-SPoxIm)$E(C_6F_5)_3$ (E = B, Al) is discussed based on experimental and theoretical results. Through this work, we directly observed the complexation-induced axial chirality around an N−P bond.

RESULTS AND DISCUSSION

Previously, we have reported the formation of (κ-*O*-PoxIm)LA or (κ-*O*-**1a**)$Al(C_6F_5)_3$ (**1a·Al**) complexes that include unreacted carbene carbons (LA is either $E(C_6F_5)_3$ (E = B[3a] and Al[4]) or MOTf (M = Li and Na)[3e]). Although the complexes were successfully isolated at room temperature when LA was $Al(C_6F_5)_3$ or MOTf, (κ-*O*-**1b**)$B(C_6F_5)_3$ (**1b·B**) was required to be characterized by NMR analysis at −90 °C, as it smoothly transformed into the thermodynamically more stable carbene−borane adduct (κ-*C*-**1b**)$B(C_6F_5)_3$ at room temperature.[3a] During our study on the complexation between (S)PoxIms

https://dx.doi.org/10.1021/acs.joc.9b03210
J. Org. Chem. 2020, 85, 14333−14341

and main group Lewis acids, and their intermediacy in the synthesis of organic/organometallic compounds, we initially examined the reaction between **1a** and $B(C_6F_5)_3$. At room temperature, we observed the quantitative formation of (κ-*O*-**1a**)$B(C_6F_5)_3$ (**1a·B**) via the coordination of the *N*-phosphinoyl group in **1a** to $B(C_6F_5)_3$ (Figure 2A). Subsequently, **1a·B** was isolated in >99% yield, and its molecular structure was unambiguously determined by NMR and single-crystal X-ray diffraction (XRD) analyses.[5] A set of (R_a) and (S_a) atropisomers of **1a·B** was identified in the asymmetric unit of the single crystal (Figure 2B).[6] The carbene carbon and *N*-phosphinoyl oxygen atoms in these atropisomers adopt an *anti*-orientation with respect to the N−P bond; however, they exhibit different C1−N1−P−O torsion angles ((R_a)-**1a·B**: +147.8(1)°, θ = +32.2°; (S_a)-**1a·B**: −147.8(1)°, θ = −32.2°). To the best of our knowledge, this is the first example of a direct observation of axial chirality generated around an N−P bond.[6b−e] Although a substantial H···F−C interaction can be expected when the H and F atoms are within a range of 2.2−2.3 Å,[7] the conformational fixation via weak H···F interactions cannot be completely ruled out in **1a·B**, as interatomic distances between a F atom in the individual C_6F_5 group and the C5−H atom of the imidazolinylidene moiety or the ^{i}Pr−H atom of the Dipp moiety are 2.577(2) or 2.670(1) Å.[8] To clarify the participation of these H···F−C interactions, the noncovalent interactions (NCIs) analysis was carried out based on the structural parameters confirmed by XRD analysis.[9] In Figure 3, NCIs observed in (R_a)-**1a·B** are represented as

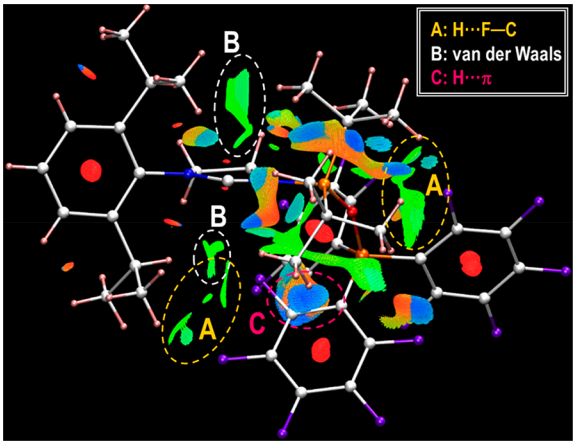

Figure 3. Visualization of the noncovalent interactions in (R_a)-**1a·B**. The cutoff value of 0.25 au is adopted for the reduced density gradient within the range of $-0.03 < \rho < 0.03$ au. Key interactions between (A) H and F atoms, (B) ^{i}Pr and ^{t}Bu groups, and (C) the H atom and the C_6F_5 ring are circled in yellow, white, and pink color, respectively.

isosurfaces colored in the blue-green-red scale, wherein regions filled in deeper blue colors suggest more attractive interactions between specific atoms and/or bonds, and deeper red colors indicate more repulsive interactions. The regions colored in green indicate weak interactions such as van der Waals and H···lone pair interactions. The H···F−C interactions between the ^{i}Pr−H and the F atoms (highlighted in the yellow cycle, Figure 3A) as well as van der Waals interactions between ^{i}Pr and the ^{t}Bu groups (highlighted in the white cycle, Figure 3B) are clearly confirmed to be involved, which would contribute to the fixation of the conformation of (R_a)-**1a·B**. In addition, NCIs such as H···F and strongly attractive CH···π (highlighted in the pink cycle, Figure 3C) interactions are also found between ^{t}Bu and C_6F_5 groups.

To gain further insight into the aforementioned axial chirality, DFT calculations were carried out at the ωB97X-D/6-311G(d,p)//ωB97X-D/6-31G(d) level of theory (gas phase; Figure 2C). In the following discussion, the relative free Gibbs energies for **TS-1a·B**, and (R_a)-**4a·B** are shown with respect to (R_a)-**1a·B** (0.0 kcal·mol^{-1}). A relaxed potential energy scan for the conversion from (R_a)-**1a·B** to(S_a)-**1a·B** via a rotation of the *N*-phosphinoyl moiety predicted the participation of the activation complex **TS-1a·B** ($\Delta G^{\ddagger}$ = $\Delta E^{\ddagger}$ = +7.6 kcal·mol^{-1}; Figure S3). In the optimized structure of **TS-1a·B**, the C1−N1−P−O torsion angle of −179.3° (θ = −0.7°) shows that these four atoms are arranged in a nearly coplanar fashion and that the steric repulsion should thus be generated between the C_6F_5 groups and the C5−H atoms of the imidazolinylidene ring (Figure 2C). On the other hand, the rotation of the *N*-phosphinoyl group in the R_a direction afforded the metastable conformer (R_a)-**4a·B** (ΔG° = +6.9 kcal·mol^{-1}; ΔE° = +6.4 kcal·mol^{-1}), which exhibits the C1−N1−P-O angle of +107.7° (θ = +72.3°; Figure 2C). Although a certain energy barrier could be predicted for the formation of (R_a)-**4a·B** based on the scanning of a potential energy surface between (R_a)-**1a·B** and (R_a)-**4a·B** (Figure S4), a structure for this transition state was not determined. Nevertheless, these results manifest that axial chirality around the N−P bond can be certainly induced to generate both (R_a)-**1a·B** as well as (S_a)-**1a·B** as the energetically most favorable species in the present system, while they should readily isomerize each other via **TS-1a·B** in solution.

In the case of free carbene **1a**, the molecular structure exhibits the C1−N1−P−O angle of 179.7(2)° (θ = 0.3°) in the crystalline state, implying that atropisomers are not generated without the complexation via the *N*-phosphinoyl group, as the rotation of *N*-phosphinoyl group in **1a** occurs without a substantial amount of energy barrier within the range of ca. $-90° \leq \theta \leq +90°$ (Figure 1A). Moreover, the corresponding axial chirality is not effectively induced even in the crystalline state of **1a·Al**; i.e., the C1−N1−P−O angles in **1a·Al** (±172.2(2)°, θ = ±7.8°) are not deviated largely from θ = 0° (Figure 2D). On the basis of these results, the aforementioned axial chirality in **1a·B** should be attributed to the restricted rotation of the *N*-phosphinoyl moieties around the N−P bonds, caused by steric repulsion between the C_6F_5 groups and the imidazolinylidene ring. In the case of **1a·Al**, the longer O−Al bond (1.786(1) Å) compared to the O−B bond (1.551(2) Å) in **1a·B** would decrease the aforementioned steric repulsion, which would enable a facile interconversion between (R_a) and (S_a) atropisomers.

The electronic structure of **1a·B** was further explored by NMR spectroscopy and an NBO analysis. The ^{31}P NMR spectrum of **1a·B** at −30 °C showed a resonance at δ_P 76.7, which is downfield shifted relative to that of **1a** (δ_P 59.6) and almost identical to that of **1a·Al** (δ_P 79.8).[4] Thus, an electron density on the phosphorus atom in **1a·B** should decrease through coordination of the *N*-phosphinoyl group to $B(C_6F_5)_3$. Furthermore, in the ^{13}C NMR spectrum, the resonance of the carbene carbon atom is observed at 245.4 ppm ($^2J_{C,P}$ = 35.5 Hz), which is almost identical to that of **1a** (δ_C 244.9; $^2J_{C,P}$ = 28.0 Hz). These results suggest (i) the enhanced electrophilicity on the phosphorus atom and (ii) the vital nucleophilicity on the carbene carbon atom in **1a·B**. The results of DFT calculations support these notions, and the

https://dx.doi.org/10.1021/acs.joc.9b03210
J. Org. Chem. 2020, 85, 14333−14341

LUMO+6 and HOMO−4 orbitals are shown together with their energy levels in Figure 4A. The energy levels of the

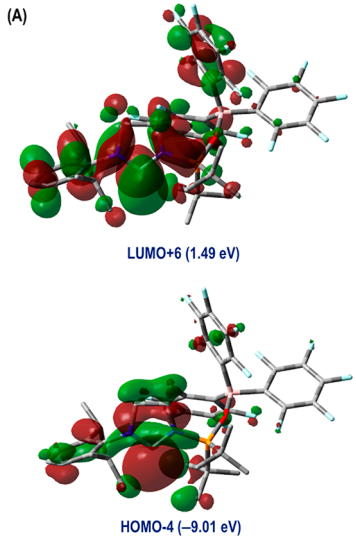

E		N–P	P–O	O–E
none	:1a	0.671	1.202	—
B	:(R_a)-1a·B	0.724	0.848	0.563
Al	:(R_a)-1a·Al	0.723	0.873	0.304

Figure 4. (A) Selected molecular orbitals of **1a·B** and their associated energy levels, calculated at the ωB97X-D/6-311G(d,p)//ωB97X-D/6-31G(d) level of theory. (B) Selected Wiberg bond indices in **1a**, (R_a)-**1a·B**, and (R_a)-**1a·Al**. Structural optimization for **1a** was conducted at the ωB97X-D/6-311G(d,p)//B3LYP/6-31G(d) level of theory.

orbitals between HOMO−1 and HOMO−4 are almost degenerate (−8.82 to −9.01 eV), and these molecular orbitals include a partial contribution of the lone pair on the carbene carbon atom (Figure S5). The contribution of the p orbital on the carbene carbon atom is observed for several energy levels, e.g., the LUMO+2 (1.16 eV) and the LUMO+6 (1.49 eV). These results are consistent with the results of the ^{13}C NMR measurements. An NBO analysis based on the Wiberg bond indices (WBIs) was carried out in order to examine the bonding situation in **1a**, (R_a)-**1a·B**, and (R_a)-**1a·Al** (Figure 4B). The bond order for the phosphinoyl P−O bond decreases from 1.202 (**1a**) to 0.848 (**1a·B**) and 0.873 (**1a·Al**), while the WBIs for the other bonds are almost identical in the **1a** moieties of these compounds (Figure S6). Nevertheless, the P−O bonds in **1a·B** and **1a·Al** are expected to possess multiple-bond character, as the P−O bond lengths observed by X-ray crystallography (**1a·B**: 1.525(1) Å; **1a·Al**: 1.521(1) Å) are still shorter than the sum of the single-bond radii of P (1.07 Å) and O (0.66 Å),[10] even though they are substantially elongated compared to the corresponding bond in **1a** (1.478(2) Å).

Complex **1a·B** gradually decomposes at room temperature (conversion of **1a·B** after 24 h: 40%), which results in the appearance of at least two resonances at δ_P 64.3 and 55.0 in the ^{31}P NMR spectrum. During this decomposition, a resonance that implies the formation of carbene−borane adduct (κ-*C*-**1a**)B(C_6F_5)$_3$ (**5a**) was not observed, based on a comparison with δ_P 76.0 of (κ-*C*-**1b**)B(C_6F_5)$_3$ (**5b**). In contrast, in the case of PoxIm **1b**, the transformation of (κ-*O*-**1b**)B(C_6F_5)$_3$ (**1b·B**) to **5b** occurred easily at room temperature.[3a] These results are rationalized in terms of the differences in the relative Gibbs free energies between the **1·B** and **5** derivatives (Figure 5). In

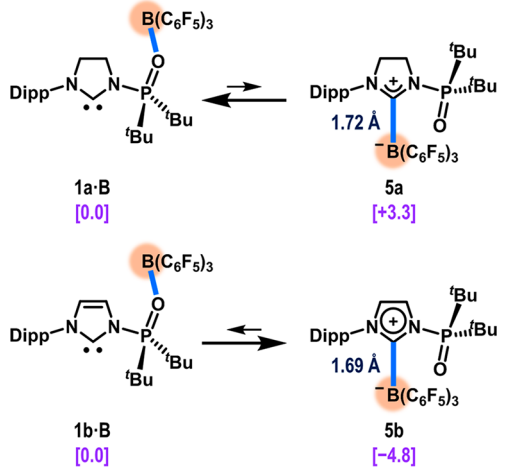

Figure 5. (A) Relative Gibbs free energies (kcal·mol^{-1}) for **5a** and **5b** are shown relative to **1a·B** and **1b·B**, respectively.

the case of **1b**, **5b** ($\Delta G°$ = −4.8 kcal·mol^{-1}) exhibits a higher stability with respect to **1b·B**, due to an effective delocalization of π-electrons over the imidazolium ring (Figure S2). In stark contrast, in the case of **1a**, **1a·B** can be expected to be energetically more favorable than **5a** ($\Delta G°$ = +3.3 kcal·mol^{-1}), probably due to a lack of the stabilization effects observed in **5b**. Moreover, the steric repulsion between the (S)PoxIm and B(C_6F_5)$_3$ moieties is expected to be higher in **5a** than that in **5b**, given the longer C−B bond (1.72 Å) in the DFT-optimized structure of **5a** compared to that in **5b** (DFT: 1.69 Å; XRD: 1.696(3) Å). A comparison of the percent buried volumes[1b,11] of **1a** (% V_{bur} = 30.8) and **1b** (% V_{bur} = 29.2) moieties in **5a** and **5b** supports that **1a** is sterically more demanding than **1b**.

Given the expected nucleophilic reactivity of the carbene carbon in **1a·B**, the reaction between **1a·B** and CO_2 (5 atm) was explored in toluene at room temperature, which resulted in the formation of **6a** in 95% isolated yield (Figure 6A-1). The molecular structure of **6a** was unambiguously determined by NMR spectroscopy and single-crystal XRD analysis (Figure 6B). Thus, CO_2 was scavenged by **1a** and B(C_6F_5)$_3$.[12] Compound **6a** might expected to be formed via the generation of imidazolium-2-carboxylate intermediate **2a·B**, in which the phosphinoyl moiety coordinates to B(C_6F_5)$_3$, followed by a transfer of B(C_6F_5)$_3$ to the carboxylate oxygen. The thermolysis of in situ generated **6a** in the presence of CO_2 (5 atm) at 100 °C for 36 h afforded (κ-*N*-**3a**)B(C_6F_5)$_3$ in 71% yield, in which the imidazole nitrogen atom of carboxylic phosphinic mixed anhydride **3a** coordinates to B(C_6F_5)$_3$. The expected accelerating effect of B(C_6F_5)$_3$ on the transformation of **1a** to **3a** was not observed under these conditions. We also carried out a reaction between **1a·Al** and CO_2 at room temperature (Figure 6A-2). The complete consumption of **1a·Al** was confirmed after 1 h, and the target (κ-*O*-**3a**)Al(C_6F_5)$_3$

https://dx.doi.org/10.1021/acs.joc.9b03210
J. Org. Chem. 2020, 85, 14333−14341

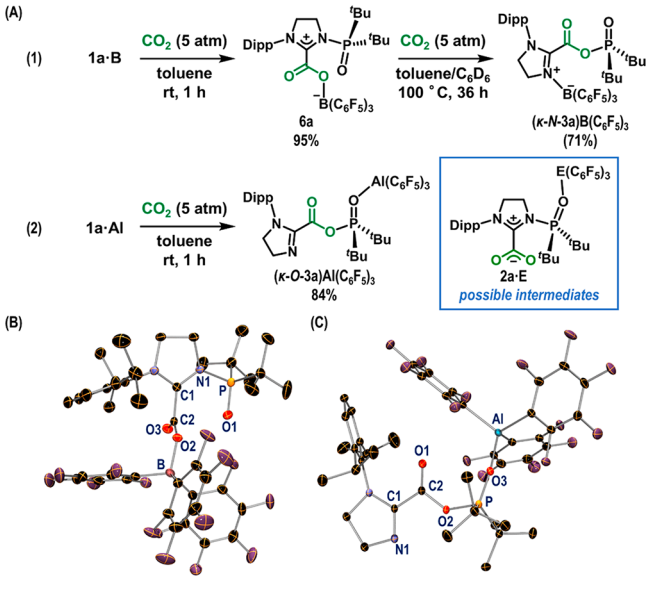

Figure 6. (A) Reaction between **1a·B**/**1a·Al** and CO_2. The isolated product yield is shown. The yield determined by NMR analysis is also shown in parentheses. (B) Molecular structure of **6a** with thermal ellipsoids at 30% probability; H atoms and a molecule of CH_2Cl_2 are omitted for clarity. Selected bond lengths (Å) and angles (deg): N1−P 1.745(2), P−O1 1.473(1), C1−C2 1.535(2), C2−O2 1.294(2), C2−O3 1.200(2), O2−B 1.540(2), C1−C2−O3 118.1(1), C1−C2−O2 110.4(1). (C) Molecular structure of (*κ-O*-**3a**)$Al(C_6F_5)_3$ with thermal ellipsoids at 30% probability; H atoms and a molecule of C_7H_8 are omitted for clarity. Selected bond lengths (Å) and angles (deg): C1−C2 1.500(5), C2−O1 1.188(4), C2−O2 1.372(3), O2−P 1.615(2), P−O3 1.507(2), O3−Al 1.795(2), C1−C2−O1 126.1(3), O1−C2−O2 123.6(3), P−O3−Al 169.4(1).

was isolated in 84% yield. The molecular structures of (*κ-N*-**3a**)$B(C_6F_5)_3$ (Figure S1) and (*κ-O*-**3a**)$Al(C_6F_5)_3$ (Figure 6C) were determined by single-crystal XRD analyses. The formation of (*κ-O*-**3a**)$Al(C_6F_5)_3$ would also proceed via an imidazolium-2-carboxylate intermediate such as **2a·Al**, followed by a migration of the activated phosphinoyl moiety.

Encouraged by the aforementioned results, we explored the room-temperature phosphinoylation of CO_2 with **1a** in the presence of a catalytic amount of Lewis acids (Figure 7). In the absence of a catalyst, **3a** was formed in 39% after 2.5 h (run 1). In the presence of $Al(C_6F_5)_3$, **3a** was formed in >99% yield (run 2), while $B(C_6F_5)_3$ did not promote the formation of **3a** (run 3). Subsequently, we examined $B(p\text{-}HC_6F_4)_3$, BPh_3, and $B(2\text{-}CF_3C_6H_4)(p\text{-}HC_6F_4)_2$ (runs 4−6), as the suppressed Lewis acidity may promote the dissociation of CO_2 from a possible resting-state compound such as **6a**. However, the yield of **3a** did not improve under these conditions. To explore the reactivity of triaryl boranes equipped with a five-membered aromatic substituent,[13,14] B(1,3-dichloroazulenyl)$(p\text{-}HC_6F_4)_2$ was employed, albeit that the improvement of the yield of **3a** was negligible (run 7, Figure 7). Al-, Ti-, and Li-based inorganic Lewis acids were also tested, which failed to accelerate the reaction (runs 8−11), probably due to the difficulty on the selective and quantitative complexation with the phosphinoyl group. It should thus be crucial to choose a suitable Lewis acid that is both sufficiently oxophilic as well as sterically demanding in order to maintain the predominant complexation via the N-phosphinoyl group in **1a** throughout the reaction.

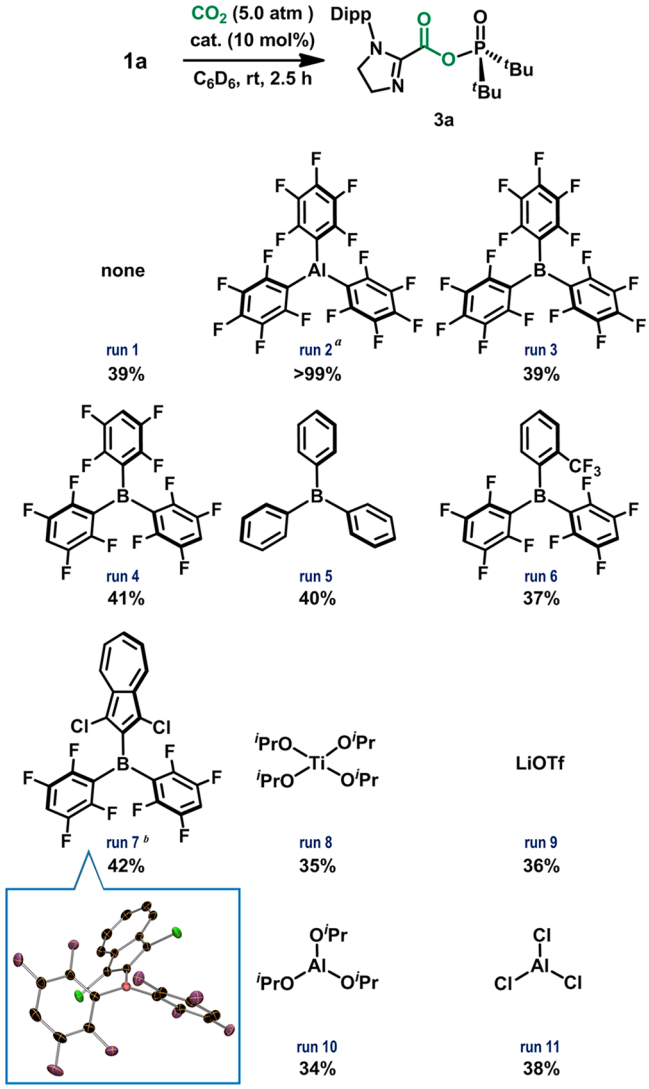

Figure 7. Reaction between **1a** and CO_2 in the presence/absence of a catalytic amount of Lewis acids. Product yields were determined by NMR spectroscopy using hexamethylbenzene as the internal standard. (a) $Al(C_6F_5)_3\cdot(tol)_{0.5}$ was used. (b) Molecular structure of B(1,3-dichloroazulenyl)$(p\text{-}HC_6F_4)_2$ with thermal ellipsoids at 30% probability.

■ CONCLUSIONS

In conclusion, we have observed the first example of complexation-induced axial chirality around an N−P bond. The complexation between $B(C_6F_5)_3$ and the *N*-phosphine oxide-substituted imidazolinylidene (SPoxIm) occurred via the predominant coordination of the *N*-phosphinoyl oxygen atom to the B center to afford the corresponding (R_a) and (S_a) atropisomers. The steric repulsion between the C5−H atoms in the imidazolinylidene ring and the C_6F_5 groups seems to be crucial for this axial chirality, as it effectively restricts the rotation of the *N*-phosphinoyl moiety. The conformational fixation via the multiple intramolecular H···F interactions as well as van der Waals interactions between alkyl groups would also contribute to the stabilization of these atropisomers. On the other hand, axial chirality was not certainly observed in the corresponding $Al(C_6F_5)_3$ complex. The vital nucleophilicity on the carbene carbon atom in (*κ-O*-SPoxIm)$B(C_6F_5)_3$ was used for the fixation of CO_2 in the corresponding carbene−CO_2−

https://dx.doi.org/10.1021/acs.joc.9b03210
J. Org. Chem. 2020, 85, 14333−14341

$B(C_6F_5)_3$ adduct that was subsequently transformed into an adduct comprising a carboxylic phosphinic mixed anhydride and $B(C_6F_5)_3$. Furthermore, in the presence of a catalytic amount of $Al(C_6F_5)_3$, the phosphinoylation of CO_2 with SPoxIm was significantly accelerated at room temperature to quantitatively afford the carboxylic phosphinic mixed anhydride, while this reaction proceeded only in moderate yields in the absence of $Al(C_6F_5)_3$. The present work showcases the multipurpose utility of strategically designed multifunctional carbenes, thus contributing to the expansion of their chemistry. Further applications of multifunctional multipurpose carbenes are currently in progress in our laboratory.

EXPERIMENTAL SECTION

General Considerations. Unless otherwise noted, all manipulations were conducted under a nitrogen atmosphere using standard Schlenk line or drybox techniques. ^{1}H, ^{11}B, ^{13}C, ^{19}F, ^{27}Al, and ^{31}P NMR spectra were recorded on a Bruker AVANCE III 400 or JEOL JNM-400 spectrometers at 25 °C. The chemical shifts in the ^{1}H NMR spectra were recorded relative to Me_4Si or residual protonated solvent (C_6D_5H (δ 7.16), toluene-d_8 (δ 7.09, 7.01, 6.97, 2.08), $CDHCl_2$ (δ 5.32), DMSO-d_6 (δ 2.50)). The chemical shifts in the ^{11}B NMR spectra were recorded relative to BF_3. The chemical shifts in the ^{13}C spectra were recorded relative to Me_4Si or deuterated solvent (C_6D_6 (δ 128.06), toluene-d_8 (δ 137.48, 128.87, 127.96, 125.13, 20.43), CD_2Cl_2 (δ 53.84), DMSO-d_6 (δ 39.52)). The chemical shifts in the ^{19}F NMR spectra were recorded relative to α,α,α-trifluorotoluene (δ −65.64). The chemical shifts in the ^{27}Al NMR spectra were recorded relative to $AlCl_3$. The chemical shifts in the ^{31}P NMR spectra were recorded relative to 85% H_3PO_4 as an external standard. Assignment of the resonances in ^{1}H and ^{13}C NMR spectra was based on ^{1}H−^{1}H COSY, HMQC, and HMBC experiments. High resolution mass spectrometry (HRMS) and elementary analyses were performed at the Instrumental Analysis Center, Faculty of Engineering, Osaka University. Exact mass spectra were recorded on a double-focusing mass spectrometer (JMS-700; JEOL). For some complexes, accurate elemental analyses were precluded by extreme air or thermal sensitivity and/or systematic problems with elemental analysis of organometallic compounds. X-ray crystal data were collected with Rigaku XtaLAB Synergy equipping with the HyPix-6000HE detector. Melting points were confirmed on a Stanford Research Systems MPA100 OptiMelt Automated Melting Point System. DFT calculations were performed using the program Gaussian 09, Revision A.02.[15] Geometry optimizations of minima and transition states were carried out without any symmetry constraint at the B3LYP or ωB97X-D level of theory[16] for 6-31G(d) basis sets. The vibrational frequencies were calculated at the ωB97X-D/6-311G(d,p) level of theory to check whether each optimized structure represents an energy minimum or a transition state, and to evaluate its zero-point vibrational energy and thermal corrections at 298.15 K (gas phase, 1 atm). All stationary-point structures were found to have the appropriate number of imaginary frequencies. The appropriateness of the connections between each reactant and product was con-firmed using quasi-intrinsic reaction coordinate (qIRC) calculations. In the qIRC calculations, the geometry of a transition state was first shifted by perturbing the geometries very slightly along the reaction coordinate, and then released for equilibrium optimization. Relative Gibbs energies were obtained by adding the Gibbs energy corrections derived from the analytical frequency calculations to the single-point energies. These calculations involve a certain margin of error.

Materials. All commercially available reagents, including super-dehydrated solvents (toluene, hexane, and Et_2O), were used as received. Benzene-d_6 and toluene-d_8 were distilled from sodium benzophenone ketyl prior to use. CD_2Cl_2 was distilled from CaH_2 and stored over molecular sieves (4 Å). Compounds **1a**,[3b] $B(p\text{-}HC_6F_4)_3$,[17a] $B(2\text{-}CF_3C_6F_4)(p\text{-}HC_6F_4)_2$,[17b] and (1,3-dichloroazulenyl)boronic acid[17c] were prepared using previously reported procedures. *Caution: $Al(C_6F_5)_3$ is a potentially explosive material, and ligand-supported derivatives such as $Al(C_6F_5)_3\cdot(tol)_{0.5}$ should thus be handled with the utmost care.*

Synthesis of Potassium Trifluoro(1,3-dichloroazulenyl)-borate. (1,3-Dichloroazulenyl)boronic acid (2.77 g, 11.5 mmol) was dissolved in methanol (20 mL) in a PE-wash bottle. The solution was treated with KHF_2 (3.60 g, 46.1 mmol, 4 equiv) dissolved in 5 mL of distilled water. The resulting suspension was stirred at room temperature for 12 h. Then extraction with acetone through a glass filter and the following removal of all volatiles at 60 °C furnished a green solid. Again extraction with acetone, filtration, and evaporation yielded a solid that was washed with hexane followed by dried in vacuo, which afforded the target product as a green solid (3.06 g, 10.1 mmol, 88%). ^{1}H NMR (400 MHz, DMSO-d_6): δ 8.15 (d, J = 9.6 Hz, 2H), 7.58 (t, J = 9.8 Hz, 1H), 7.14 (t, J = 9.8 Hz, 2H). ^{11}B NMR (128 MHz, DMSO-d_6): δ 2.0 (br). ^{13}C{^{1}H} NMR (100 MHz, DMSO-d_6): δ 138.1, 132.8, 132.0, 124.0, 122.3, 119.0. ^{19}F NMR (376 MHz, DMSO-d_6): δ −137.0 (br, 3F).HRMS(FAB$^-$): m/z calcd for $C_{10}H_5Cl_2F_3B$: ([M$^-$]) 262.9813, found 262.9816. Melting points: 230−231 °C.

Synthesis of B(1,3-dichloroazulenyl)(p-HC$_6$F$_4$)$_2$. (p-C_6F_4H)MgBr was prepared by slow addition of ^{i}PrMgCl (1.0 M in Et_2O, 7.3 mL, 7.3 mmol) to a solution of p-C_6F_4HBr (1.66 g, 7.25 mmol) in Et_2O (20 mL). The resulting mixture was stirred for 1 h at room temperature. Then (p-C_6F_4H)MgBr was added to the suspension of potassium trifluoro(1,3-dichloroazulenyl)borate (1.00 g, 3.3 mmol) in Et_2O (5 mL) at 0 °C, and the mixture was allowed to warm to room temperature with further stirring for 12 h. Then, after all volatiles were removed, the resultant mixture was extracted with 200 mL of hot hexane under N_2, followed by removal of volatiles to afford the product as a green solid (679.5 mg, 1.35 mmol, 41%). A single crystal was prepared by recrystallization from toluene/hexane at −35 °C. ^{1}H NMR (400 MHz, C_6D_6): δ 7.89 (d, J = 10.0 Hz, 2H), 6.75 (t, J = 9.8 Hz, 1H), 6.33−6.25 (m, 4H). ^{11}B NMR (128 MHz, C_6D_6): δ 62.6 (br). ^{13}C{^{1}H} NMR (100 MHz, C_6D_6): δ 147.6 (dm, $^1J_{C,F}$ = 246 Hz), 146.2 (dm, $^1J_{C,F}$ = 245 Hz), 143.3, 138.8, 134.6, 124.4, 121.1, 110.7 (t, J = 22.7 Hz). Two resonances are obscured by a C_6D_6 signal. ^{19}F NMR (376 MHz, C_6D_6): δ −133.1−133.2 (m, 2F), −141.4−141.6 (m, 2F). HRMS(EI$^+$): m/z calcd for $C_{22}H_7Cl_2F_8B$: ([M$^+$]) 503.9890, found 503.9888. Melting points: 154−155 °C. X-ray data for B(1,3-dichloroazulenyl)(p-HC_6F_4)$_2$: M = 505.02, green, monoclinic, $P2_1/c$ (#14), a = 19.1406(4) Å, b = 9.6406(2) Å, c = 11.2647(3) Å, α = 90°, β = 105.952(3)°, γ = 90°, V = 1998.60(9) Å^3, Z = 4, D_{calcd} = 1.678 g/cm^3, T = −150 °C, R_1 ($_wR_2$) = 0.0391 (0.1084).

Synthesis of 1a·B. $B(C_6F_5)_3$ (128.1 mg, 0.25 mmol) was added to a toluene solution of **1a** (97.7 mg, 0.25 mmol, 0.05 M) at room temperature. The reaction mixture was stirred for 10 min. After the removal of all volatiles in vacuo, the residue was washed with cold hexane to afford **1a·B** as a white solid (228.2 mg, 0.25 mmol, > 99%). A single crystal was prepared by recrystallization from CH_2Cl_2/hexane at −35 °C. ^{1}H NMR (400 MHz, tol-d_8, −30 °C): δ 7.15 (t, J = 7.5 Hz, 1H, Ar-*H*), 6.98 (d, J = 7.5 Hz, 2H, Ar-*H*), 3.20 (t, J = 8.8 Hz, 2H, CH_2), 2.99 (t, J = 8.8 Hz, 2H, CH_2), 2.71−2.68 (m, 2H, $CHCH_3$), 1.27 (d, J = 6.8 Hz, 6H, $CHCH_3$), 1.07 (d, J = 6.8 Hz, 6H, $CHCH_3$), 0.89 (d, $^3J_{H,P}$ = 16.4 Hz, 18H, ^{t}Bu-*H*). ^{11}B NMR (128 MHz, tol-d_8, −30 °C): δ −2.7 (br). ^{13}C{^{1}H} NMR (100 MHz, tol-d_8, −30 °C): δ 245.4 (d, $^2J_{C,P}$ = 35.5 Hz, NCN), 148.6 (dm, $^1J_{C,F}$ = 240 Hz), 145.7, 140.3 (dm, $^1J_{C,F}$ = 245 Hz), 137.5 (dm, $^1J_{C,F}$ = 246 Hz), 137.1, 136.6, 124.2, 120.2 (br), 53.2, 49.3, 39.3 (d, $^1J_{C,P}$ = 68.6 Hz), 28.7, 26.7, 25.2, 23.0. ^{19}F NMR (376 MHz, tol-d_8, −30 °C): δ −131.3 (s, 6F), −156.8 (m, 3F), −163.7 (m, 6F). ^{31}P{^{1}H} NMR (162 MHz, tol-d_8, −30 °C): δ 76.7 (s). Anal. Calcd for $C_{41}H_{39}BF_{15}N_2OP$: C, 54.56; H, 4.36; N, 3.10. Found: C, 54.40; H, 4.32; N, 3.20. Melting points: 145−146 °C. X-ray data for **1a·B**: M = 902.55, colorless, triclinic, P-1 (#2), a = 10.6793(2) Å, b = 11.2817(2) Å, c = 16.7507(4) Å, α = 86.433(2)°, β = 84.296(2)°, γ = 88.897(2)°, V = 2004.08(7) Å^3, Z = 2, D_{calcd} = 1.495 g/cm^3, T = −150 °C, R_1 ($_wR_2$) = 0.0336 (0.0879).

Reaction between 1a·B and CO$_2$. A 10 mL autoclave was charged with **1a·B** (190.5 mg, 0.21 mmol) and toluene (6.0 mL). Once sealed, the vessel was pressurized with CO_2 (5 atm), and the

https://dx.doi.org/10.1021/acs.joc.9b03210
J. Org. Chem. 2020, 85, 14333−14341

reaction mixture was stirred at room temperature for 1 h. After the removal all volatiles in vacuo, the residue was washed with cold hexane to afford **6a** as a white solid (190.2 mg, 0.20 mmol, 95%). A single crystal was prepared by recrystallization from CH_2Cl_2/hexane at −35 °C. ^{1}H NMR (400 MHz, CD_2Cl_2): δ 7.47 (t, J = 7.9 Hz, 1H, Ar-*H*), 7.22 (d, J = 7.9 Hz, 2H, Ar-*H*), 4.34 (t, J = 8.8 Hz, 2H, CH_2), 4.27−4.25 (m, 2H, CH_2), 2.86 (br, 2H, $CHCH_3$), 1.39 (d, $^3J_{H,P}$ = 15.6 Hz, 18H, ^{t}Bu-*H*), 1.20 (d, J = 6.8 Hz, 12H, $CHCH_3$). ^{11}B NMR (128 MHz, CD_2Cl_2): δ −2.5 (br). ^{13}C{^{1}H} NMR (100 MHz, CD_2Cl_2): δ 151.9 (s, OCO), 148.6 (dm, $^1J_{C,F}$ = 227 Hz), 146.4, 137.0 (dm, $^1J_{C,F}$ = 250 Hz), 132.2, 129.4, 128.7 (d, $^2J_{C,P}$ = 19.0 Hz, NCN), 125.4, 55.9, 49.1, 38.9 (d, $^1J_{C,P}$ = 63.0 Hz), 29.6, 27.0, 26.7, 22.6. Several resonances for the C_6F_5 ring were not identified. ^{19}F NMR (376 MHz, CD_2Cl_2): δ −134.3 (d, J = 18.8 Hz, 6F), −165.3 (t, J = 20.7 Hz, 6F), −170.6 (t, J = 18.8 Hz, 6F). ^{31}P{^{1}H} NMR (162 MHz, CD_2Cl_2): δ 68.9 (s). Anal. Calcd for $C_{42}H_{39}BF_{15}N_2O_3P{\cdot}CH_2Cl_2$: C, 50.07; H, 4.01; N, 2.72. Found: C, 48.74; H, 3.79; N, 2.80. X-ray data for **6a**·CH_2Cl_2: M = 1031.50, colorless, monoclinic, $P2_1/n$ (#14), a = 10.5340(3) Å, b = 21.0599(6) Å, c = 20.8720(6) Å, α = 90°, β = 95.002(2)°, γ = 90°, V = 4612.7(2) Å^3, Z = 4, D_{calcd} = 1.485 g/cm^3, T = −150 °C, R_1 ($_wR_2$) = 0.0397 (0.0951).

Thermolysis of 6a in the Presence of CO_2. A pressure-tight NMR tube (Wilmad-LabGlass, 524-PV-7) was charged with **1a·B** (15.7 mg, 0.017 mmol) and toluene/C_6D_6 (0.5 mL, v/v = 4/1). Once sealed, the mixture was pressurized with CO_2 (5 atm), confirming the quantitative generation of **6a**. This reaction mixture was heated at 100 °C for 36 h. After the removal all volatiles in vacuo, the residue was washed with hexane to afford a crude mixture (13.3 mg) which includes (*κ-N*-**3a**)$B(C_6F_5)_3$ in 71% (0.012 mmol; determined by ^{31}P NMR analysis). The formation of (*κ-N*-**3a**)$B(C_6F_5)_3$ was unambiguously confirmed by the comparison with the authentic compound that was prepared by the reaction between **3a** and $B(C_6F_5)_3$ in toluene. ^{1}H NMR (400 MHz, CD_2Cl_2): δ 7.40 (t, J = 7.7 Hz, 1H, Ar-*H*), 7.23 (d, J = 7.7 Hz, 2H, Ar-*H*), 4.38 (br, 2H, CH_2), 4.06 (t, J = 10.6 Hz, 2H, CH_2), 3.02 (br, 2H, $CHCH_3$), 1.29 (d, J = 20.4 Hz, 6H, $CHCH_3$), 1.21 (d, J = 6.8 Hz, 6H, $CHCH_3$), 0.86 (d, $^3J_{H,P}$ = 16.8 Hz, 18H, ^{t}Bu-*H*). ^{11}B NMR (128 MHz, CD_2Cl_2): δ −8.1 (br). ^{13}C{^{1}H} NMR (100 MHz, CD_2Cl_2): δ 158.9, 152.9 (d, $^2J_{C,P}$ = 10 Hz), 149.2 (dm, $^1J_{C,F}$ = 242 Hz), 148.2, 140.5 (dm, $^1J_{C,F}$ = 262 Hz), 137.6 (dm, $^1J_{C,F}$ = 241 Hz), 131.8, 130.5, 125.7, 53.7, 52.3, 38.0 (d, $^1J_{C,P}$ = 69 Hz), 32.0, 29.2, 26.9, 26.5. Resonances for the *ipso*-carbons of C_6F_5 ring were not identified. ^{19}F NMR (376 MHz, CD_2Cl_2): δ −132.2 (d, J = 15.0 Hz, 2F), −135.1−135.4 (m, 2F), −136.4 (d, J = 15.0 Hz, 2F), −160.9 (t, J = 21.7 Hz, 1F), −161.9−162.3 (m, 2F), −162.9 (t, J = 22.6 Hz, 1F), −167.1 (br, 2F), −167.7 (br, 2F), −168.9 (t, J = 16.9 Hz, 1F). ^{31}P{^{1}H} NMR (162 MHz, CD_2Cl_2): δ 84.7 (s). Anal. Calcd for $C_{42}H_{39}BF_{15}N_2O_3P$: C, 53.30; H, 4.15; N, 2.96. Found: C, 53.81; H, 4.51; N, 2.95. Melting points: 151−152 °C. X-ray data for (*κ-N*-**3a**)$B(C_6F_5)_3$: M = 946.56, colorless, monoclinic, $P2_1/c$ (#14), a = 12.5964(5) Å, b = 21.5652(12) Å, c = 18.5448(9) Å, α = 90°, β = 95.214(4)°, γ = 90°, V = 5016.7(4) Å^3, Z = 4, D_{calcd} = 1.253 g/cm^3, T = 25 °C, R_1 ($_wR_2$) = 0.0676 (0.2225).

Reaction between 1b·Al and CO_2. A 50 mL autoclave was charged with **1b·Al** (79.0 mg, 0.086 mmol) and toluene (2.0 mL). Once sealed, the vessel was pressurized with CO_2 (5 atm), and the reaction mixture was stirred at room temperature for 1 h. After the removal all volatiles in vacuo, the residue was washed with cold hexane to afford (*κ-O*-**3a**)$Al(C_6F_5)_3$ as a white solid (69.7 mg, 0.072 mmol, 84%). A single crystal was prepared by recrystallization from toluene/hexane at −35 °C. ^{1}H NMR (400 MHz, C_6D_6): δ 7.19 (t, J = 7.6 Hz, 1H, Ar-*H*), 6.98 (d, J = 7.6 Hz, 2H, Ar-*H*), 3.69 (t, J = 11.3 Hz, 2H, CH_2), 3.24 (t, J = 11.3 Hz, 2H, CH_2), 2.98−2.91 (m, 2H, $CHCH_3$), 1.15 (d, J = 6.8 Hz, 6H, $CHCH_3$), 1.07 (d, J = 6.8 Hz, 6H, $CHCH_3$), 0.97 (d, $^3J_{H,P}$ = 17.2 Hz, 18H, ^{t}Bu-*H*). ^{13}C{^{1}H} NMR (100 MHz, C_6D_6): δ 150.5 (dm, $^1J_{C,F}$ = 233 Hz), 147.2, 141.8 (dm, $^1J_{C,F}$ = 247 Hz), 137.3 (dm, $^1J_{C,F}$ = 230 Hz), 134.1, 132.3, 129.5, 124.5, 54.8, 54.1, 37.6 (d, $^1J_{C,P}$ = 73 Hz), 28.6, 25.3, 24.9, 23.8. Resonances for the *ipso*-carbons of C_6F_5 ring and NCN were not identified. ^{19}F NMR (376 MHz, C_6D_6): δ −124.5−124.6 (m, 6F), −157.0 (t, J = 18.8 Hz, 3F), −165.3−165.4 (m, 6F). ^{27}Al NMR (103 MHz, C_6D_6): δ 113.1 (br, $\nu_{1/2}$ = ca. 4000 Hz). ^{31}P{^{1}H} NMR (162 MHz, C_6D_6): δ 79.5 (br). In the case of (*κ-O*-**3a**)$Al(C_6F_5)_3$, an accurate elemental analysis was precluded by extreme air sensitivity and/or systematic problems with elemental analysis of organometallic compounds: Anal. Calcd for $C_{42}H_{39}AlF_{15}N_2O_3P$: C, 52.40; H, 4.08; N, 2.91. Found: C, 50.91; H, 3.90; N, 3.09. Melting points: 118−119 °C. X-ray data for (*κ-O*-3a)$Al(C_6F_5)_3{\cdot}C_7H_8$: M = 1054.86, colorless, triclinic, P-1 (#2), a = 11.0128(3) Å, b = 12.0642(3) Å, c = 20.6781(6) Å, α = 83.247(2)°, β = 75.607(2)°, γ = 66.202(3)°, V = 2434.35(13) Å^3, Z = 2, D_{calcd} = 1.439 g/cm^3, T = −150 °C, R_1 ($_wR_2$) = 0.0557 (0.1544).

General Procedures for the Reaction between 1a and CO_2 in the Presence/Absence of a Catalyst. A pressure-tight NMR tube (Wilmad-LabGlass, 524-PV-7) was charged with **1a** (0.04 mmol), additive (0.004 mmol, 10 mol %), hexamethylbenzene (0.04 mmol; an internal standard for NMR analysis), and C_6D_6 (0.4 mL). Once sealed, the tube was pressurized with CO_2 (5 atm), and the reaction was monitored by ^{1}H NMR at room temperature.

Noncovalent Interactions (NCIs) Analysis for (R_a)-1a·B. NCI analysis was carried out based on the structural parameters (xyz coordinates) obtained by the single-crystal XRD analysis of (R_a)-**1a·B**. A profile for the reduced density gradient (RDG < 1.0 au) was prepared as a function of electron density (ρ) multiplied by the sign of the Hessian second eigenvalue, sign(λ_2)ρ, with the NCIPLOT program (Figure S7).[9] On the basis of this result, the isosurfaces shown in Figure 3 are visualized with the VMD program[18] by adopting the cutoff values of RDG = 0.25 au and −0.03 < ρ < 0.03 au. These surfaces are colored according to the indicated sign(λ_2)ρ values: blue colors suggest more attractive interactions; deeper red colors indicate more repulsive interactions; green colors indicate weak interactions.

■ ASSOCIATED CONTENT

Supporting Information

The Supporting Information is available free of charge at https://pubs.acs.org/doi/10.1021/acs.joc.9b03210.

NMR spectra, molecular structure of (*κ-N*-**3a**)$B(C_6F_5)_3$, details on experimental procedures for Figure 6, the DFT calculations (NCI analysis), and calculated Cartesian coordinates(PDF)

X-ray data for obtained compounds (CIF)

■ AUTHOR INFORMATION

Corresponding Authors

Yoichi Hoshimoto − *Osaka University, Suita, Japan;* orcid.org/0000-0003-0882-6109; Email: hoshimoto@chem.eng.osaka-u.ac.jp

Sensuke Ogoshi − *Osaka University, Suita, Japan;* orcid.org/0000-0003-4188-8555; Email: ogoshi@chem.eng.osaka-u.ac.jp

Other Authors

Takahiro Asada − *Osaka University, Suita, Japan*

Takahiro Kawakita − *Osaka University, Suita, Japan*

Takuya Kinoshita − *Osaka University, Suita, Japan*

Complete contact information is available at: https://pubs.acs.org/10.1021/acs.joc.9b03210

Notes

The authors declare no competing financial interest.

■ ACKNOWLEDGMENTS

This work was supported by a Grant-in-Aid for Young Scientists (JSPS KAKENHI grant JP18K14219) and the Grant-in-Aid for Scientific Research on Innovative Areas

"Precisely Designed Catalysts with Customized Scaffolding (JSPS KAKENHI grant JP15H05803)." T.A. would like to express his gratitude for a Grant-in-Aid for JSPS Fellows.

REFERENCES

(1) For recent reviews, see: (a) Hopkinson, M. N.; Richter, C.; Schedler, M.; Glorius, F. An Overview of *N*-Heterocyclic Carbenes. *Nature* **2014**, *510*, 485−496. (b) Gómez-Suárez, A.; Nelson, D. J.; Nolan, S. P. Quantifying and Understanding the Steric Properties of *N*-Heterocyclic Carbenes. *Chem. Commun.* **2017**, *53*, 2650−2660. (c) Smith, C. A.; Narouz, M. R.; Lummis, P. A.; Singh, I.; Nazemi, A.; Li, C. H.; Crudden, C. M. *N*-Heterocyclic Carbenes in Materials Chemistry. *Chem. Rev.* **2019**, *119*, 4986−5056.

(2) For recent reviews, see: (a) Gaillard, S.; Renaud, J. L. When Phosphorus and NHC (*N*-Heterocyclic Carbene) Meet Each Other. *Dalton Trans.* **2013**, *42*, 7255−7270. (b) Kuwata, S.; Hahn, F. E. Complexes Bearing Protic*N*-Heterocyclic Carbene Ligands. *Chem. Rev.* **2018**, *118*, 9642−9677. (c) Peris, E. Smart *N*-Heterocyclic Carbene Ligands in Catalysis. *Chem. Rev.* **2018**, *118*, 9988−10031. (d) Danopoulos, A. A.; Simler, T.; Braunstein, P. *N*-Heterocyclic Carbene Complexes of Copper, Nickel, and Cobalt. *Chem. Rev.* **2019**, *119*, 3730−3961. (e) Doddi, A.; Peters, M.; Tamm, M. *N*-Heterocyclic Carbene Adducts of Main Group Elements and Their Use as Ligands in Transition Metal Chemistry. *Chem. Rev.* **2019**, *119*, 6994−7112.

(3) (a) Hoshimoto, Y.; Kinoshita, T.; Ohashi, M.; Ogoshi, S. A Strategy to Control the Reactivation of Frustrated Lewis Pairs from Shelf-Stable Carbene Borane Complexes. *Angew. Chem., Int. Ed.* **2015**, *54*, 11666−11671. (b) Hoshimoto, Y.; Asada, T.; Hazra, S.; Kinoshita, T.; Sombut, P.; Kumar, R.; Ohashi, M.; Ogoshi, S. Strategic Utilization of Multifunctional Carbene for Direct Synthesis of Carboxylic-Phosphinic Mixed Anhydride from CO_2. *Angew. Chem., Int. Ed.* **2016**, *55*, 16075−16079. (c) Hoshimoto, Y.; Asada, T.; Hazra, S.; Ohashi, M.; Ogoshi, S. Phosphorylation of Isocyanates and Aldehydes Mediated by Multifunctional *N*-Phosphine Oxide-Substituted Imidazolylidenes. *Chem. Lett.* **2017**, *46*, 1211−1213. (d) Hazra, S.; Hoshimoto, Y.; Ogoshi, S. *N*-Phosphine Oxide-Substituted Imidazolylidenes (PoxIms): Multifunctional Multipurpose Carbenes. *Chem. - Eur. J.* **2017**, *23*, 15238−15243. (e) Kinoshita, T.; Sakuraba, M.; Hoshimoto, Y.; Ogoshi, S. Complexation between MOTf (M = Li and Na) and *N*-Phosphine Oxide-Substituted Imidazolylidenes via Coordination of the *N*-Phosphoryl Groups. *Chem. Lett.* **2019**, *48*, 230−233.

(4) Asada, T.; Hoshimoto, Y.; Ogoshi, S. *Complexation between Al(C_6F_5)$_3$ and N-Phosphine Oxide-Substituted Imidazolidenes, 3F-C-3 in 27th*; International Society of Heterocyclic Chemistry Congress, Kyoto, 2019. Details for the synthetic procedure, identification, and reactivity will be reported in due course.

(5) For details, see the Supporting Information.

(6) (a) For a recent example on a complexation-induced axial chirality on NHC complexes, see: Kong, L.; Morvan, J.; Pichon, D.; Jean, M.; Albalat, M.; Vives, T.; Colombel-Rouen, S.; Giorgi, M.; Dorcet, V.; Roisnel, T.; Crévisy, C.; Nuel, D.; Nava, P.; Humbel, S.; Vanthuyne, N.; Mauduit, M.; Clavier, H. From Prochiral*N*-Heterocyclic Carbenes (NHC) to Optically Pure Metal Complexes: New Opportunities in Asymmetric Catalysis. *J. Am. Chem. Soc.* **2019**, DOI: 10.1021/jacs.9b12698. (b) For recent reviews on axial chirality, see: Kumarasamy, E.; Raghunathan, R.; Sibi, M. P.; Sivaguru, J. Nonbiaryl and Heterobiaryl Atropisomers: Molecular Templates with Promise for Atropselective Chemical Transformations. *Chem. Rev.* **2015**, *115*, 11239−11300. (c) Smyth, J. E.; Butler, N. M.; Keller, P. A. A Twist of Nature-the Significance of Atropisomers in Biological Systems. *Nat. Prod. Rep.* **2015**, *32*, 1562−1583. (d) Glunz, P. W. Recent Encounters with Atropisomerism in Drug Discovery. *Bioorg. Med. Chem. Lett.* **2018**, *28*, 53−60. (e) Toenjes, S. T.; Gustafson, J. L. Atropisomerism in Medicinal Chemistry: Challenges and Opportunities. *Future Med. Chem.* **2018**, *10*, 409−422.

(7) (a) Dunitz, J. D.; Taylor, R. Organic Fluorine Hardly Ever Accepts Hydrogen Bonds. *Chem. - Eur. J.* **1997**, *3*, 89−98. (b) Doerrer, L. H.; Green, M. L. Oxidation of [M(η-C_5H_5)$_2$], M = Cr, Fe or Co, by the new Brønsted acid $H_2O\eta B(C_6F_5)_3$ yielding the salts [M(η-C_5H_5)$_2$]$^+$A$^-$, where A$^-$ = [(C_6F_5)$_3$B(μ-OH)B(C_6F_5)$_3$]$^-$ or [(C_6F_5)$_3$BOH···H_2OB(C_6F_5)$_3$]$^-$. *J. Chem. Soc., Dalton Trans.* **1999**, 4325−4329. (c) Mountford, A. J.; Hughes, D. L.; Lancaster, S. J. Intra- and Inter-Molecular C-H···F-C and N-H···F-C Hydrogen Bonding in Secondary Amine Adducts of $B(C_6F_5)_3$: Relevance to Key Interactions in Alkene Polymerisation Catalysis. *Chem. Commun.* **2003**, *3*, 2148−2149. (d) Lancaster, S. J.; Mountford, A. J.; Hughes, D. L.; Schormann, M.; Bochmann, M. Ansa-Metallocenes with B-N and B-P Linkages: The Importance of N-H···F-C Hydrogen Bonding in Pentafluorophenyl Boron Compounds. *J. Organomet. Chem.* **2003**, *680*, 193−205. (e) Mountford, A. J.; Lancaster, S. J.; Coles, S. J.; Horton, P. N.; Hughes, D. L.; Hursthouse, M. B.; Light, M. E. Intra- and Intermolecular N-H···F-C Hydrogen-Bonding Interactions in Amine Adducts of Tris(Pentafluorophenyl)Borane and -Alane. *Inorg. Chem.* **2005**, *44*, 5921−5933.

(8) For a discussion on HHHHF interactions up to ca. 2.8 Å in the crystalline state, see: (a) Thalladi, V. R.; Weiss, H. C.; Bläser, D.; Boese, R.; Nangia, A.; Desiraju, G. R. C-H···F Interactions in the Crystal Structures of Some Fluorobenzenes. *J. Am. Chem. Soc.* **1998**, *120*, 8702−8710. (b) Vangala, V. R.; Nangia, A.; Lynch, V. M. Interplay of Phenyl-Perfluorophenyl Stacking, C-H···F, C-F···π and F···F Interactions in Some Crystalline Aromatic Azines. *Chem. Commun.* **2002**, 1304−1305. (c) Kui, S. C. F.; Zhu, N.; Chan, M. C. W. Observation of Intramolecular C-H···F-C Contacts in Non-Metallocene Polyolefin Catalysts: Model for Weak Attractive Interactions between Polymer Chain and Noninnocent Ligand. *Angew. Chem., Int. Ed.* **2003**, *42*, 1628−1632. (d) Althoff, G.; Ruiz, J.; Rodríguez, V.; López, G.; Pérez, J.; Janiak, C. Can a Single C-H···F-C Hydrogen Bond Make a Difference? Assessing the H···F Bond Strength from 2-D ^{1}H-^{19}F CP/MAS NMR. *CrystEngComm* **2006**, *8*, 662−665.

(9) (a) Johnson, E. R.; Keinan, S.; Mori-Sánchez, P.; Contreras-García, J.; Cohen, A. J.; Yang, W. Revealing Noncovalent Interactions. *J. Am. Chem. Soc.* **2010**, *132*, 6498−6506. (b) Contreras-García, J.; Johnson, E. R.; Keinan, S.; Chaudret, R.; Piquemal, J. P.; Beratan, D. N.; Yang, W. NCIPLOT: A Program for Plotting Noncovalent Interaction Regions. *J. Chem. Theory Comput.* **2011**, *7*, 625−632.

(10) Cordero, B.; Gómez, V.; Platero-Prats, A. E.; Revés, M.; Echeverría, J.; Cremades, E.; Barragán, F.; Alvarez, S. Covalent Radii Revisited. *Dalton Trans.* **2008**, 2832−2838.

(11) The % V_{bur} values were calculated using the Samb*V*ca program with the following parameters: sphere radius, 3.00 Å; distance for the metal−ligand bond, 2.00 Å; H atoms were omitted; Bondi radii were scaled by 1.17. For this program, see: (a) Poater, A.; Cosenza, B.; Correa, A.; Giudice, S.; Ragone, F.; Scarano, V.; Cavallo, L. Samb*V* ca: A Web Application for the Calculation of the Buried Volume of *N*-Heterocyclic Carbene Ligands. *Eur. J. Inorg. Chem.* **2009**, *2009*, 1759−1766. (b) Falivene, L.; Credendino, R.; Poater, A.; Petta, A.; Serra, L.; Oliva, R.; Scarano, V.; Cavallo, L. Samb*V* ca 2. A Web Tool for Analyzing Catalytic Pockets with Topographic Steric Maps. *Organometallics* **2016**, *35*, 2286−2293.

(12) For recent reviews on CO_2 fixation by frustrated Lewis pairs comprising carbenes and triarylboranes, see: (a) Stephan, D. W.; Erker, G. Frustrated Lewis Pair Chemistry of Carbon, Nitrogen and Sulfur Oxides. *Chem. Sci.* **2014**, *5*, 2625−2641. (b) Stephan, D. W.; Erker, G. Frustrated Lewis Pair Chemistry: Development and Perspectives. *Angew. Chem., Int. Ed.* **2015**, *54*, 6400−6441. (c) Weicker, S. A.; Stephan, D. W. Main Group Lewis Acids in Frustrated Lewis Pair Chemistry: Beyond Electrophilic Boranes. *Bull. Chem. Soc. Jpn.* **2015**, *88*, 1003−1016. (d) Fontaine, F. G.; Courtemanche, M. A.; Légaré, M. A.; Rochette, É. Design Principles in Frustrated Lewis Pair Catalysis for the Functionalization of Carbon Dioxide and Heterocycles. *Coord. Chem. Rev.* **2017**, *334*, 124−135. (e) Jupp, A. R.; Stephan, D. W. New Directions for Frustrated Lewis Pair Chemistry. *Trends Chem.* **2019**, *1*, 35−48.

https://dx.doi.org/10.1021/acs.joc.9b03210
J. Org. Chem. 2020, 85, 14333−14341

(13) Tao, X.; Daniliuc, C. G.; Soloviova, K.; Strassert, C. A.; Kehr, G.; Erker, G. Arylallenes and the Halogeno-B$(C_6F_5)_2$ Reagents: Facile Formation of 2-Borylindenes. *Chem. Commun.* **2019**, *55*, 10166−10169.
(14) B(1,3-dichloroazulenyl)(p-$HC_6F_4)_2$ exhibits a slightly lower (ca. 5%) Lewis acidity toward $Et_3P{=}O$ compared to B$(C_6F_5)_3$, which was confirmed by the Gutmann−Beckett method. For details, see the Supporting Information.
(15) *Gaussian 09*, Revision A.02: Frisch, M. J.; Trucks, G. W.; Schlegel, H. B.; Scuseria, G. E.; Robb, M. A.; Cheeseman, J. R.; Scalmani, G.; Barone, V.; Mennucci, B.; Petersson, G. A.; Nakatsuji, H.; Caricato, M.; Li, X.; Hratchian, H. P.; Izmaylov, A. F.; Bloino, J.; Zheng, G.; Sonnenberg, J. L.; Hada, M.; Ehara, M.; Toyota, K.; Fukuda, R.; Hasegawa, J.; Ishida, M.; Nakajima, T.; Honda, Y.; Kitao, O., Nakai, H.; Vreven, T.; Montgomery, J. A., Jr.; Peralta, J. E.; Ogliaro, F.; Bearpark, M.; Heyd, J. J.; Brothers, E.; Kudin, K. N.; Staroverov, V. N; Kobayashi, R.; Normand, J.; Raghavachari, K.; Rendell, A.; Burant, J. C.; Iyengar, S. S.; Tomasi, J.; Cossi, M.; Rega, N.; Millam, J. M.; Klene, M.; Knox, J. E.; Cross, J. B.; Bakken, V.; Adamo, C.; Jaramillo, J.; Gomperts, R.; Stratmann, R. E.; Yazyev, O.; Austin, A. J.; Cammi, R.; Pomelli, C.; Ochterski, J. W.; Martin, R. L.; Morokuma, K.; Zakrzewski, V. G.; Voth, G. A.; Salvador, P.; Dannenberg, J. J.; Dapprich, S.; Daniels, A. D.; Farkas, O.; Foresman, J. B.; Ortiz, J. V.; Cioslowski, J.; Fox, D. J. Gaussian, Inc., Wallingford, CT, 2009.
(16) Chai, J.-D.; Head-Gordon, M. Long-Range Corrected Hybrid Density Functionals with Damped Atom-Atom Dispersion Corrections. *Phys. Chem. Chem. Phys.* **2008**, *10*, 6615−6620.
(17) (a) Ullrich, M.; Lough, A. J.; Stephan, D. W. Reversible, Metal-Free, Heterolytic Activation of H_2 at Room Temperature. *J. Am. Chem. Soc.* **2009**, *131*, 52−53. (b) Hoshimoto, Y.; Kinoshita, T.; Hazra, S.; Ohashi, O.; Ogoshi, S. Main-Group-Catalyzed Reductive Alkylation of Multiply Substituted Amines with Aldehydes Using H_2. *J. Am. Chem. Soc.* **2018**, *140*, 7292−7300. (c) Kurotobi, K.; Tabata, H.; Miyauchi, M.; Mustafizur, R. A. F. M.; Migita, K.; Murafuji, T.; Sugihara, Y.; Shimoyama, H.; Fujimori, K. The First Generation of Azulenyl-Lithium and -Magnesium: A Novel, Versatile Method of Introducing a Substituent at the 2-Position of an Azulene Skeleton. *Synthesis* **2003**, *1*, 30−34.
(18) Humphrey, W.; Dalke, A.; Schulten, K. VMD: Visual Molecular Dynamics. *J. Mol. Graphics* **1996**, *14*, 33−38.

https://dx.doi.org/10.1021/acs.joc.9b03210
J. Org. Chem. 2020, 85, 14333−14341